20. Beck, S. L. & Ruff, L. J. Rupture process of the great 1963 Kuril Islands earthquake sequence: asperity interaction and multiple event rupture. *J. Geophys. Res.* **92**, 14123–14138 (1987).

21. Kanamori, H. Mechanism of tsunami earthquakes. *Phys. Earth Planet. Inter.* **6**, 246–259 (1972).

22. Okal, E. A. & Newman, A. V. Tsunami earthquakes: The quest for a regional signal. *Phys. Earth Planet. Inter.* **124**, 45–70 (2001).

23. Tanioka, Y. & Satake, K. Fault parameters of the 1896 Sanriku tsunami earthquake estimated from tsunami numerical modeling. *Geophys. Res. Lett.* **23**, 1549–1552 (1996).

24. Thatcher, W. Earthquake recurrence and risk assessment in circum-Pacific seismic gaps. *Nature* **341**, 432–434 (1989).

25. Schwartz, S. Y. Noncharacteristic behavior and complex recurrence of large subduction zone earthquakes. *J. Geophys. Res.* **104**, 23111–23125 (1999).

26. Ando, M. Source mechanisms and tectonic significance of historical earthquakes along the Nankai trough. *Japan. Tectonophysics* **27**, 119–140 (1975).

27. Mansinha, L. & Smyle, D. E. The displacement fields of inclined faults. *Bull. Seismol. Soc. Am.* **61**, 1433–1440 (1971).

28. Imamura, F. in *Long-wave Runup Models* (eds Yeh, H., Liu, P. & Synolakis, C.) 25–42 (World Scientific, Singapore, 1996).

29. Satake, K. Linear and nonlinear computations of the 1992 Nicaragua earthquake tsunami. *Pure Appl. Geophys.* **144**, 455–470 (1995).

30. Iwasaki, T. & Mano, A. Two-dimensional numerical simulation of tsunami run-ups in the Eulerian description [in Japanese]. *Proc. 26th Conf. Coastal Eng. JSCE*, 70–72 (Japan Soc. Civil Engineers, Tokyo, 1979).

....

The hydrodynamics of water strider locomotion

David L. Hu[1], **Brian Chan**[2] & **John W. M. Bush**[1]

[1]*Department of Mathematics, and*
[2]*Department of Mechanical Engineering MIT, Cambridge, Massachusetts 02139, USA*

....

Water striders *Gerridae* are insects of characteristic length 1 cm and weight 10 dynes that reside on the surface of ponds, rivers, and the open ocean[1–4]. Their weight is supported by the surface tension force generated by curvature of the free surface[5,6], and they propel themselves by driving their central pair of hydrophobic legs in a sculling motion[7,8]. Previous investigators have assumed that the hydrodynamic propulsion of the water strider relies on momentum transfer by surface waves[1,9,10]. This assumption leads to Denny's paradox[11]: infant water striders, whose legs are too slow to generate waves, should be incapable of propelling themselves along the surface. We here resolve this paradox through reporting the results of high-speed video and particle-tracking studies. Experiments reveal that the strider transfers momentum to the underlying fluid not primarily through capillary waves, but rather through hemispherical vortices shed by its driving legs. This insight guided us in constructing a self-contained mechanical water strider whose means of propulsion is analogous to that of its natural counterpart.

Whereas substantial advances have been made in the field of biolocomotion[9,12–16], the hydrodynamics underlying the surface locomotion of semiaquatic insects remains poorly understood[1,9,11,17]. There are two means of walking on water according to the relative magnitudes of the body weight Mg and the maximum curvature force σP, where M is the body mass, g the gravitational acceleration, σ the surface tension and P the contact perimeter of the water-walker[17]. Water-walkers characterized by $M_c = \frac{Mg}{\sigma P} > 1$, such as the basilisk lizard, rely on the force generated by their feet slapping the surface and propelling water downward[18]. Creatures with $M_c < 1$, such as the water strider may reside at rest on the surface, supported by the curvature force generated by distortion of the free surface (Fig. 1). The body and legs of the water strider are covered by thousands of hairs[1] that render its legs effectively non-wetting[19]. During their rowing stroke, water striders drive their middle legs against the water without penetrating the surface and may achieve peak speeds of $150 \, \text{cm s}^{-1}$. The striders may launch themselves with a vertical component, or glide along the surface.

The force balance on a stationary water strider may be understood in terms of the statics of floating, non-wetting bodies[6]. The weight of a stationary water strider is supported by some combination of the buoyancy force, F_b, and the curvature force, F_c, associated with the surface tension σ : $Mg = F_b + F_c$. F_b is deduced by integrating the hydrostatic pressure over the body area in contact with the water, while F_c is deduced by integrating the curvature pressure over this area, or equivalently the vertical component of the surface tension, $\sigma \sin\theta$, along the contact perimeter (Fig. 1b). Keller[6] demonstrated that the ratio of F_b to F_c is equal to that of the fluid volumes displaced inside and outside the contact line. For a long thin water-strider leg, this ratio is $F_b/F_c \sim w/L_c \ll 1$, where $w \approx 40 \, \mu\text{m}$ is the leg radius[1], $L_c = (\sigma/\rho g)^{1/2} \approx 2 \, \text{mm}$ the capillary length, and ρ the density of water. The strider's weight is supported almost exclusively by surface tension. Figure 2 illustrates the dependence of the maximum surface tension force on body weight for 342 species of water striders. The observed dependence illustrates that as the striders increase in size, their legs become proportionately longer. It is only thus that the largest water strider (marked C in Fig. 2), *Gigantometra gigas*[20], whose length may exceed 20 cm, is a viable water-walker.

For the water strider to move, Newton's third law requires that it transfer momentum to the underlying fluid. It has previously been assumed that capillary waves are the sole means by which to accomplish this momentum transfer[1,9–11]. Denny[9] suggested that the leg speed of the infant water strider is less than the minimum phase speed of surface waves[21], $c_m = (4g\sigma/\rho)^{1/4} \approx 23.2 \, \text{cm s}^{-1}$; consequently, the infants are incapable of generating waves and so transferring momentum to the underlying fluid. According to this physical picture, infant water striders cannot swim, an inference referred to as Denny's paradox[9,11].

A series of laboratory experiments were conducted in order to elucidate the hydrodynamic propulsion mechanism of the water strider *Gerris remigis*. Water striders were collected from local freshwater ponds and maintained in aquaria. The striders reproduced every several weeks, providing the opportunity to study the first-instar nymph water striders in a laboratory setting. The striders were filmed using a high-speed video camera at 500 frames per second and the images were digitized and analysed using Midas motion analysis software. Particle tracking was performed by seeding water with either Kalliroscope or Pliolite particles of size 50–100 μm. Dye studies were performed using food colouring and thymol blue. Images of the waves and vortices generated by the strider motion were obtained from both plan and side views; their form and speed were measured directly following the stroke. The surface signature of the capillary waves was measured with a technique adopted from Schooley[22].

The Reynolds number characterizing the adult leg stroke is $\text{Re} = UL_2/\nu \approx 10^3$, where $U \approx 100 \, \text{cm s}^{-1}$ is the peak leg speed and $L_2 \approx 0.3 \, \text{cm}$ is the length of the rowing leg's tarsal segment (see Figs 1b and 2), which prescribes the size of the dynamic meniscus forced by the leg stroke[23]. For the 0.01-s duration of the stroke, the driving legs apply a total force $F \approx 50$ dynes, the magnitude of

663

letters to nature
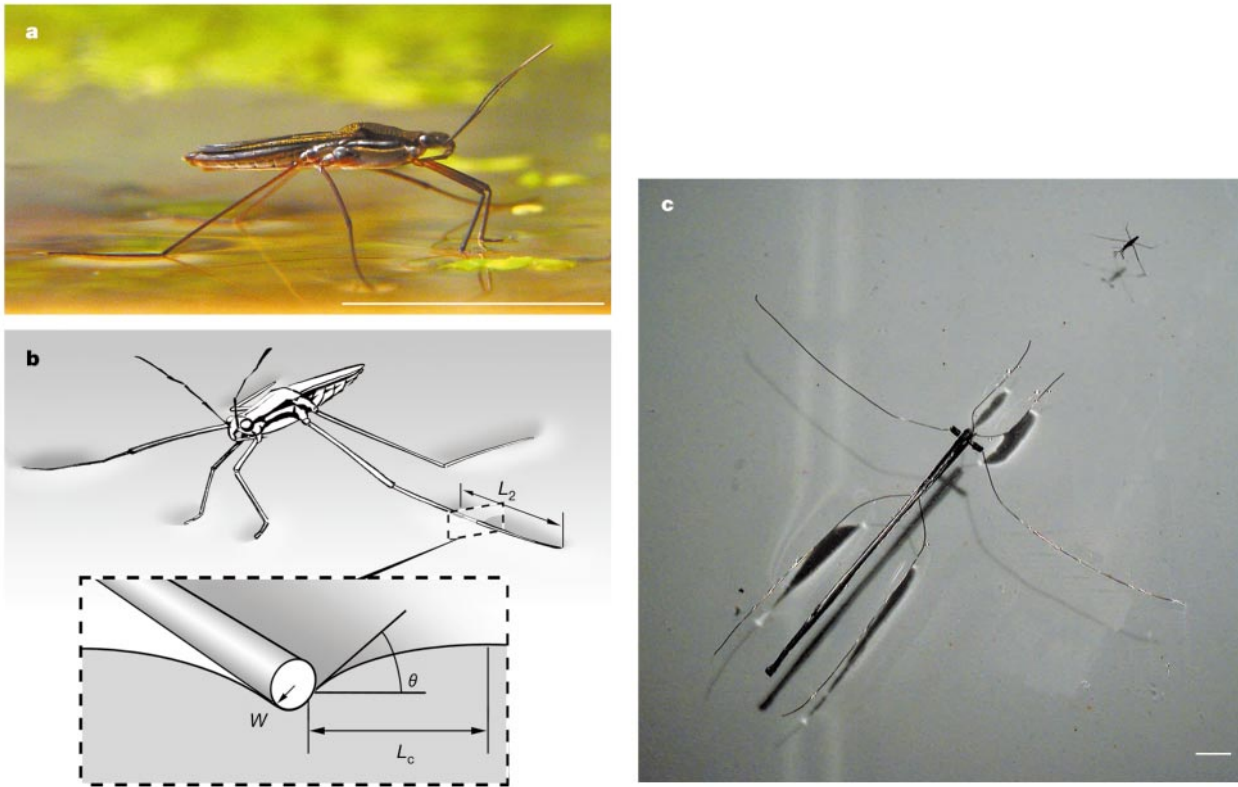
Figure 1 Natural and mechanical water striders. **a**, An adult water strider *Gerris remigis*. **b**, The static strider on the free surface, distortion of which generates the curvature force per unit leg length $2\sigma \sin \theta$ that supports the strider's weight. **c**, An adult water strider facing its mechanical counterpart. Robostrider is 9 cm long, weighs 0.35 g, and has proportions consistent with those of its natural counterpart. Its legs, composed of 0.2-mm gauge stainless steel wire, are hydrophobic and its body was fashioned from lightweight aluminium. Robostrider is powered by an elastic thread (spring constant 310 dynes cm^{-1}) running the length of its body and coupled to its driving legs through a pulley. The resulting force per unit length along the driving legs is 55 dynes cm^{-1}. Scale bars, 1 cm.
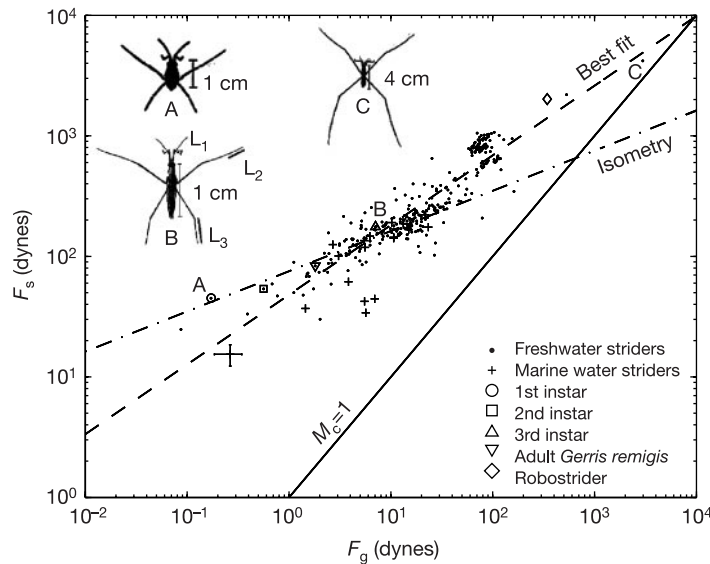
Figure 2 The relation between maximum curvature force $F_s = \sigma P$ and body weight $F_g = Mg$ for 342 species of water striders. σ is the surface tension of either pond water (67 dynes cm^{-1}) or sea water[17] (78 dynes cm^{-1}) at 14 °C and $P = 4(L_1 + L_2 + L_3)$ is twice the combined lengths of the tarsal segments (see strider B). Anatomical measurements were compiled from existing data[20,26–29]. Open symbols denote striders observed in our laboratory. Insets show the adult *Gerris remigis* (B) and extremes in size: the first-instar infant *Gerris remigis* (A) and the *Gigantometra gigas*[20] (C). The solid line represents $M_c = 1$, the minimum requirement for static stability on the surface. The surface tension force is more than adequate to support the water strider's weight; however, the margin of safety (the distance above $M_c = 1$) decreases with increasing body size. If the proportions of the water strider were independent of its characteristic size L, one would expect $P \sim L$ and hence $F_s \sim L$, and $F_g \sim L^3$: isometry would thus suggest $F_s \sim F_g^{1/3}$, a relation indicated by the dash-dotted line. The best fit to the data is given by $F_s = 48F_g^{0.58}$ (dashed line). Characteristic error bars are shown.
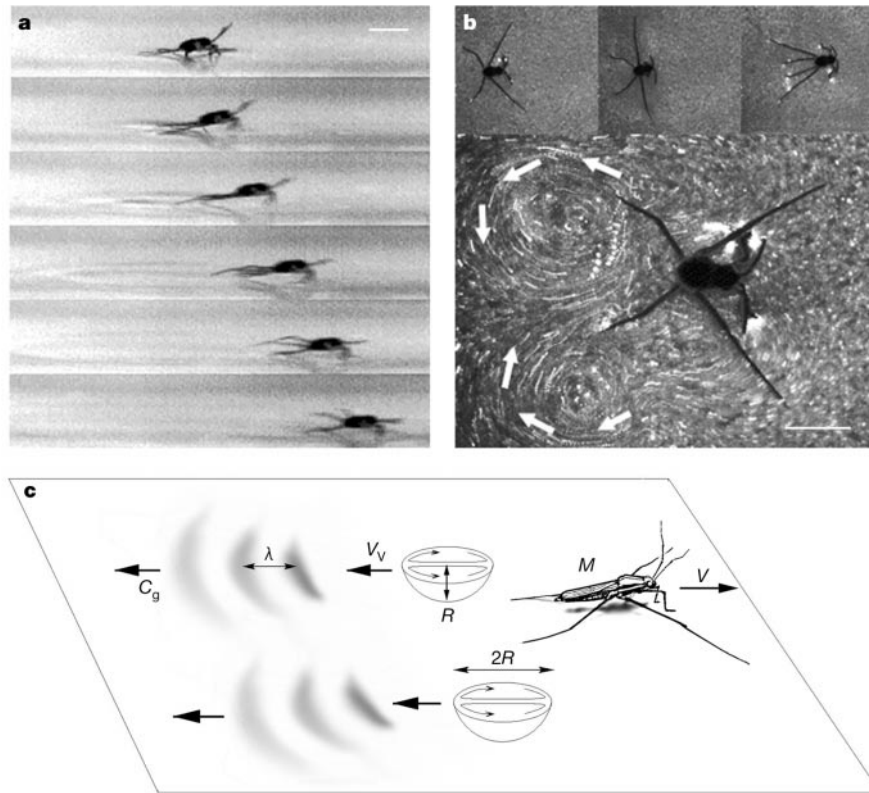
Figure 3 The flow generated by the driving stroke of the water strider. **a**, **b**, The stroke of a one-day-old first-instar water strider. Sequential images were taken 0.016 s apart. **a**, Side view. Note the weak capillary waves evident in its wake. **b**, Plan view. The underlying flow is rendered visible by suspended particles. For the lowermost image,

fifteen photographs taken 0.002 s apart were superimposed. Note the vortical motion in the wake; the flow direction is indicated. The strider legs are cocked for the next stroke. Scale bars, 1 mm. **c**, A schematic illustration of the flow structures generated by the driving stroke: capillary waves and subsurface hemispherical vortices.

which was deduced independently by measuring the strider's acceleration and leaping height. The applied force per unit length along its driving legs is thus approximately $50/0.6 \approx 80$ dynes cm^{-1}. An applied force per unit length in excess of $2\sigma \approx 140$ dynes cm^{-1} will result in the strider penetrating the free surface. The water strider is thus ideally tuned to life at the water surface: it applies as great a force as possible without jeopardizing its status as a water-walker.

The propulsion of a one-day-old first-instar is detailed in Fig. 3. Particle tracking reveals that the infant strider transfers momentum to the fluid through dipolar vortices shed by its rowing motion. The wake of the adult water strider is similarly marked by distinct vortex dipole pairs that translate backwards at a characteristic speed $V_v \approx 4$ cm s^{-1} (Figs 3c and 4). Video images captured from a side view indicate that the dipolar vortices are roughly hemispherical, with a characteristic radius $R \approx 0.4$ cm. The vertical extent of the hemispherical vortices greatly exceeds the static meniscus depth[24], 120 µm, but is comparable to the maximum penetration depth of the meniscus adjoining the driving leg, 0.1 cm. A strider of mass $M \approx 0.01$ g achieves a characteristic speed $V \approx 100$ cm s^{-1} and so has a momentum $P = MV \approx 1$ g cm s^{-1}. The total momentum in the pair of dipolar vortices of mass $M_v = 2\pi R^3/3$ is $P_v = 2M_v V_v \approx 1$ g cm s^{-1}, and so comparable to that of the strider.

The leg stroke may also produce a capillary wave packet, whose contribution to the momentum transfer may be calculated. We consider linear monochromatic deep-water capillary waves with surface deflection $\zeta(x,t) = ae^{i(kx-\omega t)}$ propagating in the x-direction with a group speed $c_g = d\omega/dk$, phase speed $c = \omega/k$, amplitude a, wavelength $\lambda = 2\pi/k$ and lateral extent W. The time-averaged horizontal momentum associated with a single wavelength,

$P_w = \pi\sigma k a^2 W c^{-1}$, may be computed from the velocity field and relations between wave kinetic energy and momentum[21,25]. Our measurements indicate that the leg stroke typically generates a wave train consisting of three waves with characteristic wavelength $\lambda \approx 1$ cm, phase speed $c \approx 30$ cm s^{-1}, amplitude $a \approx 0.01$–0.05 cm, and width $L_2 \approx 0.3$ cm (see Fig. 3c). The net momentum carried by the capillary wave packet thus has a maximum value $P_w \approx 0.05$ g cm s^{-1}, an order of magnitude less than the momentum of the strider.

The momentum transported by vortices in the wake of the water strider is comparable to that of the strider, and greatly in excess of that transported in the capillary wave field; moreover, the striders are capable of propelling themselves without generating discernible capillary waves. We thus conclude that capillary waves do not play an essential role in the propulsion of *Gerridae*, and thereby circumvent Denny's paradox. The strider generates its thrust by rowing, using its legs as oars and its menisci as blades. As in the case of rowing boats, while waves are an inevitable consequence of the rowing action, they do not play a significant role in the momentum transfer necessary for propulsion. We note that their mode of propulsion relies on the Reynolds number exceeding a critical value of approximately 100, suggesting a bound on the minimum size of water striders. Our continuing studies of water strider dynamics will follow those of birds, insects and fish[11,15,16] in characterizing the hydrodynamic forces acting on the body through detailed examination of the flows generated during the propulsive stroke.

We designed a mechanical water strider, Robostrider, constructed to mimic the motion of a water strider (Fig. 1c). Its proportions and M_c value were consistent with those of its natural counterpart
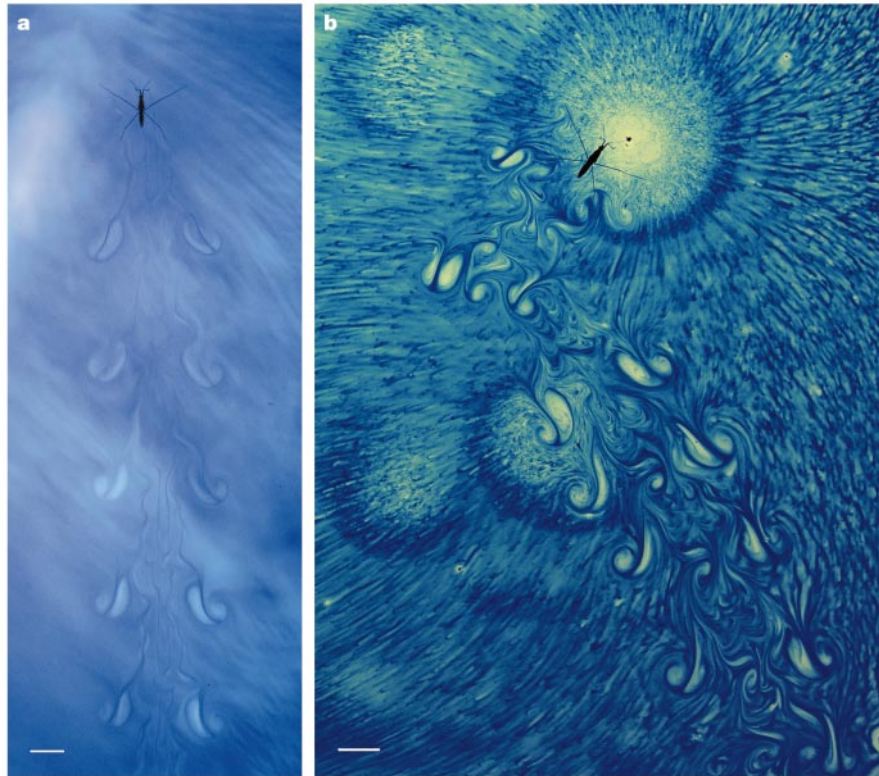
Figure 4 Dipolar vortices in the wake of the adult water strider. Images captured from a side view indicate their hemispherical form. **a**, A thin layer (2–5 mm) of thymol blue was established on the surface of the water, disturbance of which revealed the vortical footprints of the water strider. **b**, The ambient texture results from Marangoni convection[30] in the suspending fluid prompted by thymol blue on its surface. The starburst pattern results from the chunk of thymol blue evident at its centre reducing the local surface tension, thus driving surface divergence that sweeps away the dyed surface layer. The fluid is illuminated from below; consequently, the light-seeking water strider is drawn to the starbursts. Scale bars, 1 cm.

(Fig. 2). The challenge was constructing a self-contained device sufficiently light to be supported by surface tension and capable of rowing without breaking the water surface. An important design criterion, that the force per unit length along the driving legs not exceed 2σ, was met by appropriate choice of elastic thread and pulley. High-speed video footage indicates that Robostrider does not break the surface despite leg speeds of $18\,\text{cm}\,\text{s}^{-1}$. Like its natural counterpart, the Robostrider generates both capillary waves and vortices, and the principal momentum transfer is in the form of vortices shed by the rowing motion. Robostrider travels half a body length per stroke in a style less elegant than its natural counterpart. ☐

1. Andersen, N. M. A comparative study of locomotion on the water surface in semiaquatic bugs (Insecta, Hemiptera, Gerromorpha). *Vidensk. Meddr. Dansk. Naturh. Foren.* **139,** 337–396 (1976).
2. Brinkhurst, R. O. Studies on the functional morphology of *Gerris najas degeer* (Hem. Het. Gerridae). *Proc. Zool. Soc. Lond.* **133,** 531–559 (1960).
3. Murphey, R. K. A: Motor control of orientation to prey by the water strider *Gerris remigis*. *Z. Vergl. Physiol.* **72,** 150–167 (1971).
4. Wilcox, R. S. Sex discrimination in *Gerris remigis*: Role of a surface wave signal. *Science* **206,** 1325–1327 (1979).
5. Baudoin, R. La physico-chimie des surfaces dans la vie des arthropodes aeriens des miroirs d'eau, des rivages marins et lacustres et de la zone intercotidale. *Bull. Biol. Fr. Belg.* **89,** 16–164 (1955).
6. Keller, J. B. Surface tension force on a partly submerged body. *Phys. Fluids* **10,** 3009–3010 (1998).
7. Darnhofer-Demar, B. Zur Fortbewegung des Wasserlaufers *Gerris lacustris* L. auf des Wasseroberflache. *Zool. Anz. Suppl.* **32,** 430–439 (1969).
8. Bowdan, E. Walking and rowing in the water strider, *Gerris remigis*. *J. Comp. Physiol.* **123,** 43–49 (1978).
9. Denny, M. W. *Air and Water: The Biology and Physics of Life's Media* (Princeton Univ. Press, Princeton, NJ, 1993).
10. Sun, S. M. & Keller, J. B. Capillary-gravity wave drag. *Phys. Fluids* **13,** 2146–2151 (2001).
11. Suter, R. B., Rosenberg, O., Loeb, S., Wildman, H. & Long, J. H. Locomotion on the water surface: propulsive mechanisms of the fisher spider *Dolomedes triton*. *J. Exp. Biol.* **200,** 2523–2538 (1997).
12. Childress, S. *Mechanics of Swimming and Flying* (Cambridge Univ. Press, Cambridge, UK, 1981).
13. Vogel, S. *Life's Devices* (Princeton Univ. Press, Princeton, NJ, 1988).
14. Dickinson, M. H. *et al.* How animals move: an integrated view. *Science* **288,** 100–106 (2000).
15. Rayner, J. M. V., Jones, G. & Thomas, A. Vortex flow visualizations reveal change in upstroke function with flight speed in bats. *Nature* **321,** 162–164 (1986).
16. Ellington, C. P. Oxygen consumption of bumblebees in forward flight. *Nature* **347,** 472–473 (1990).
17. Vogel, S. *Life in Moving Fluids* (Princeton Univ. Press, Princeton, NJ, 1994).
18. Glasheen, J. W. & McMahon, T. A. A hydrodynamic model of locomotion in the Basilisk Lizard. *Nature* **380,** 340–342 (1996).
19. de Gennes, P.-G., Brochard-Wyart, F. & Quere, D. *Gouttes, Boules, Perles et Ondes* (Belin, Collection Echelles, Paris, 2002).
20. Tseng, M. & Rowe, L. Sexual dimorphism and allometry in the giant water strider *Gigantometra gigas*. *Can. J. Zool.* **77,** 923–929 (1999).
21. Lamb, H. *Hydrodynamics*, 6th edn (Cambridge Univ. Press, Cambridge, 1932).
22. Schooley, A. H. Profiles of wind-created water waves in the capillary-gravity transition region. *J. Mar. Res.* **16,** 100–108 (1958).
23. Suter, R. B. & Wildman, H. Locomotion on the water surface: hydrodynamic constraints on rowing velocity require a gait change. *J. Exp. Biol.* **202,** 2771–2785 (1999).
24. Matsuda, K., Watanabe, S. & Eiju, T. Real-time measurement of large liquid surface deformation using a holographic shearing interferometer. *Appl. Opt.* **24,** 4443–4447 (1985).
25. Starr, V. P. Momentum and energy integrals for gravity waves of finite height. *J. Mar. Res.* **6,** 175–193 (1947).
26. Andersen, N. M. *The Semiaquatic Bugs (Hemiptera, Gerromorpha): Phylogeny, Adaptations, Biogeography and Classification* (Scandinavian Science, Klampenborg, 1982).
27. Hungerford, H. B. & Matsuda, R. Keys to subfamilies, tribes, genera and subgenera of the *Gerridae* of the world. *Kans. Univ. Sci. Bull.* **41** (1960).
28. Henry, T. J. & Froeschner, R. C. (eds) *Catalog of the Heteroptera, of True Bugs, of Canada and the Continental United States* (E. J. Brill, Leiden, 1998).
29. Cobben, R. H. The Hemiptera of the Netherlands. *Stud. Fauna Curacao Caribb. Islands* **11,** 1–34 (1960).
30. Scriven, L. E. & Sternling, C. V. The Marangoni effects. *Nature* **187,** 186–188 (1970).